

Kirchhoff scattering from non-penetrable targets modeled as an assembly of triangular facets

Ahmad T. Abawi^{a)}

Heat, Light, and Sound Research, Inc., 12625 High Bluff Drive, Suite 211, San Diego, California 92130, USA

(Received 12 February 2016; revised 16 August 2016; accepted 25 August 2016; published online 21 September 2016)

Frequency and time domain solutions for the scattering of acoustic waves from an arbitrarily shaped target using the Kirchhoff approximation are developed. In this method, the scattering amplitude is analytically evaluated on a single triangle and scattering from a triangularly faceted target is computed by coherently summing the contributions from all the triangles that make up its surface. In the frequency domain, the solution is expressed in terms of regular (non-singular) functions, which only require the knowledge of the directions of the incident and scattered fields, the edge vectors for the triangles and position vectors to one of their vertices. To derive representations using regular functions in the time domain, the scattered signal is expressed by different expressions for various limiting cases. The frequency domain solution is validated by comparing its results to the solutions of problems for which the Kirchhoff approximation has analytic solutions. In order of increasing complexity, they include the square plate, the circular plate, the finite cylinder and the sphere. The time domain solution is validated by comparing it to the time domain solution of the Kirchhoff approximation for a rigid sphere. © 2016 Acoustical Society of America.

[<http://dx.doi.org/10.1121/1.4962735>]

[JFL]

Pages: 1878–1886

I. INTRODUCTION

The Kirchhoff approximation is a mathematical representation of Huygen's principle.¹ It can be derived from the Helmholtz-Kirchhoff integral equation by replacing the unknown field quantities at a point on the surface of the scatterer by those that would be present on an infinite tangent plane at that point. The nature of this approximation naturally excludes scattering from the shadowed regions of the scatterer, but despite this seemingly crude approximation, the Kirchhoff approximation has been a powerful technique in computing high frequency scattering both in acoustics and electromagnetics for well over a hundred years.

One of the difficulties associated with the Kirchhoff approximation is due to the complexity that arises in performing a surface integral over an arbitrary surface. One way of overcoming this difficulty is to approximate the surface with smaller facets, be it curved or flat. Nonuniform rational B-spline surfaces² is an example of curved facets, but the disadvantage of these is that at best they provide an approximate solution even on a single facet. The use of planar facets, which lend themselves to analytic solutions, is more popular. Sammelman³ and George and Bahl⁴ used rectangular facets, but their shortcoming is that they cannot properly represent an arbitrarily shaped curved surface. Furthermore, they are just a special case of the more versatile and powerful triangular facets.

Fawcett⁵ derived an analytical expression for backscattering from a plane triangular facet in the frequency domain and used the inverse Fourier transform to obtain an analytic representation of this formulation in the time domain, but

both versions of this formulation contain terms that can become singular unless appropriate limits are taken. The emergence of singularities in this process is not physical, but solely a mathematical artifact that arises because a smooth object is approximated by planar facets. This means that there is always a way to remove them, but the process of removing these singularities, which results in conditions for the range of applicability of the formulation, proves cumbersome and can significantly slow down computation.

Wendelboe *et al.*⁸ essentially derived the same formulation as Fawcett's,⁵ but they manipulated their formula to obtain one that has one singular term instead of three. And even though they show that the singular term has a limit, one would have to switch to a different formula in this limit. Considering that an object can be composed of a huge number of triangles, the process of finding triangles with a singular term and replacing the scattering formula for those triangles can be significantly time consuming.

In this paper, we derive an analytic expression for the scattering amplitude in the frequency domain for a single planar triangle. This can be used to compute scattering from a compact object meshed by triangular facets by coherently summing the contributions from all the triangles that make up its surface. The most important features of our formulation are (1) it does not contain any singular terms and (2) it is expressed in terms coordinate-independent parameters, which only requires the edge vectors for the triangles, the direction of the incident and scattered fields and a position vector to one of the vertices of the triangles. In our formulation, we have been able to represent the singular term by a well-behaved sinc-like function. In addition to this, we derive a time domain version of this formulation, which is also free of singularities. While the frequency domain version of the

^{a)}Electronic mail: abawi@hlsresearch.com

formulation can be expressed by a single formula, its time domain representation must be represented by different formulas for various limiting cases. For this reason, the frequency domain formulation is computationally more efficient. It must be noted that this model is designed to approximate the Kirchhoff scattering integral for a non-penetrable object. For this reason, its accuracy can only be judged on how well it agrees with the Kirchhoff approximation. Therefore, to validate it, we compare its solution with that of the Kirchhoff approximation for cases which the latter has analytic or close-form solutions. This way the possibility of numerical error in the reference solution is minimized. Ordered in increasing degree of complexity, we validate the model for a square plate, a circular plate, a finite cylinder and a sphere.

This paper is organized as follows: We derive the frequency domain formulation in the first part and the time domain formulation in the second part of Sec. II. In Sec. III, we present various examples to validate the two formulations. This is followed by a summary in Sec. IV.

II. MODEL DERIVATION

In the first part of this section we derive the scattering amplitude using the Kirchhoff approximation for a single triangle. We express the formula in terms of the directions of the incident and scattered fields, the edge vectors for the triangle and a position vector to one of its vertices. We manipulate the formula to express it in terms of regular functions and remove the singularities that stem from approximating a surface by planar facets. Equation (7) is the main result of this paper. In the second half of this section, we derive an analytic formula for scattering of a signal from a triangle in the time domain by taking the inverse Fourier transform of Eq. (7). To express this formulation in terms of regular functions, we derive different representations for various limiting cases. They are given by Eqs. (14) and (16).

A. Frequency domain representation of the scattering amplitude

In the far-field, the scattered field is given by⁶

$$p_s(\vec{x}) = T(\vec{k}, \vec{q}) \frac{e^{ikr}}{r}, \quad (1)$$

where \vec{k} is the incoming wave vector, \vec{q} is the outgoing wave vector defined by $\vec{q} \equiv \hat{x}k$, \vec{x} is the coordinates of the receiver, $r = |\vec{x}|$ and the scattering amplitude T valid in the Kirchhoff approximation is given by⁷

$$T(\vec{k}, \vec{q}) = \mp \frac{i}{4\pi} \int_S (\hat{n} \cdot \vec{Q}) e^{i\vec{Q} \cdot \vec{x}'} d^2x', \quad \vec{x}' \in S. \quad (2)$$

In the above formula and throughout the paper the upper sign is for the Dirichlet (soft) boundary condition and the lower sign is for the Neumann (hard) boundary condition, S is the surface of the scatterer, \hat{n} is the outward unit normal to S and $\vec{Q} = \vec{k} - \vec{q}$.

To obtain the scattering amplitude for an object whose surface can be represented by a triangular mesh, we use the above formula to obtain an analytic expression for a single triangle. The scattering amplitude for the object is then obtained by coherently adding the contributions from all the triangles that make up its surface. The scattering amplitude in the local coordinate system of a triangle shown in Fig. 1 can be written as

$$T(\vec{k}, \vec{q}) = \mp \frac{iQ_z}{4\pi} \int_0^c \int_{by/c}^{a+(b-a)y/c} e^{i(Q_x x + Q_y y)} dx dy,$$

which after some manipulations integrates to

$$T(\vec{k}, \vec{q}) = \mp \frac{Q_z c}{4\pi Q_x} e^{iaQ_x/2} \times \left\{ e^{i(cQ_y + bQ_x)/2} \text{sinc}[(cQ_y + (b-a)Q_x)/2] - e^{i(cQ_y + (b-a)Q_x)/2} \text{sinc}[(cQ_y + bQ_x)/2] \right\}, \quad (3)$$

where $\text{sinc}(x) = \sin(x)/x$. Referring to Fig. 1, we can write

$$\begin{aligned} aQ_x &= \vec{Q} \cdot \vec{T}_{12}, \\ (b-a)Q_x + cQ_y &= \vec{Q} \cdot \vec{T}_{23}, \\ bQ_x + cQ_y &= -\vec{Q} \cdot \vec{T}_{31}, \end{aligned}$$

where the edge vectors \vec{T}_{12} , \vec{T}_{23} , and \vec{T}_{31} are numbered according to the vertices of the triangle, which are numbered in the counterclockwise direction. This allows Eq. (3) to be written in terms of coordinate independent parameters for a triangle in three-dimensions whose vertex 1 is a distance R from the center of the coordinate system

$$T(\vec{k}, \vec{q}) = \mp \frac{A\vec{Q} \cdot \hat{n}}{2\pi\vec{Q} \cdot \vec{T}_{12}} e^{i\vec{Q} \cdot \vec{R}} e^{i\vec{Q} \cdot \vec{T}_{12}/2} \times \left[e^{-i\vec{Q} \cdot \vec{T}_{31}/2} \text{sinc}(\vec{Q} \cdot \vec{T}_{23}/2) - e^{-i\vec{Q} \cdot \vec{T}_{23}/2} \text{sinc}(\vec{Q} \cdot \vec{T}_{31}/2) \right]. \quad (4)$$

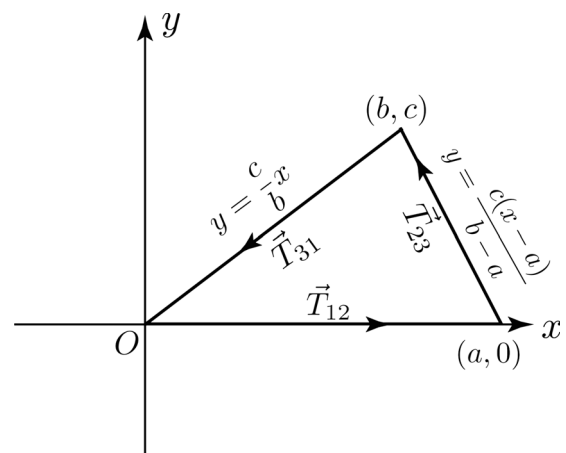


FIG. 1. The triangle used in deriving the scattering amplitude formula.

In the above formula, \hat{n} is the outward unit normal to the surface of the triangle, $A = ac/2$ is its area and Q_z has been replaced by $\vec{Q} \cdot \hat{n}$, and in deriving the above formula use has been made of the identity $\vec{T}_{12} + \vec{T}_{23} + \vec{T}_{31} = 0$.

Equation (4) expresses the scattering amplitude, $T(\vec{k}, \vec{q})$, from a single triangle described by its three edge vectors, the unit normal to its surface and a position vector \vec{R} . The edge vectors and the unit normal to the surface can be computed once the coordinates of the three vertices are specified. This formula summed over all ensonified triangles on the surface of an object gives the Kirchhoff integral, Eq. (2), exactly for any flat object with straight edges and becomes an approximation for flat objects with curved edges and for objects with curved surfaces. While in the former case, it is sufficient to represent the surface by as few triangles as possible, in the latter cases the accuracy of the model increases by increasing the number of triangles. To enforce the condition that the sum should only include ensonified triangle, $\hat{n} \cdot \vec{k} < 0$ and $\hat{n} \cdot \vec{q} > 0$ must be satisfied for each ensonified triangle.

Equation (4) is equivalent to, but a simpler form of Eq. (14a) of Wendelboe *et al.*,⁸ expressed in terms coordinate independent parameters. Equation (25) of Fawcett⁵ can also be brought to a similar form. However, a quick examination of Eq. (25) of Fawcett's shows that it can become singular when the denominators of any of the three terms go to zero. This happens when both \vec{k} and \vec{q} are perpendicular to any edges of any of the triangles making up the surface of the object. And considering that the object can be made up of a huge number of triangles, this is not such an unlikely scenario. These singularities obviously have no physical significance and are mathematical artifacts, resulting from approximating a surface by planar facets. For this reason they can be removed by taking the appropriate limits. However, the process of taking the limits can be cumbersome and often results in expressions that can still possess singularities, requiring further regularization.

In deriving Eq. (4) and Eq. (14a) of Wendelboe *et al.*,⁸ some effort has been made to get rid of the singular terms, but the terms $\vec{Q} \cdot \vec{T}_{12}$ in Eq. (4) and b in Eq. (14a) of Wendelboe *et al.*⁸ can still go to zero, causing their respective equations to become singular. Taking the limit of Eq. (4) for $\vec{Q} \cdot \vec{T}_{12} \rightarrow 0$ results in

$$T(\vec{k}, \vec{q}) = \mp \frac{A\vec{Q} \cdot \hat{n}}{2\pi} e^{i\vec{Q} \cdot \vec{R}_0} \mathcal{B}, \quad (5)$$

where

$$\mathcal{B} \equiv \left[\frac{i}{2} \text{sinc}^2(\vec{Q} \cdot \vec{T}_{31}/2) + \text{sinc}(\vec{Q} \cdot \vec{T}_{31}/2) \right. \\ \left. \times \sin(\vec{Q} \cdot \vec{T}_{31}/2) - \frac{\text{sinc}(\vec{Q} \cdot \vec{T}_{31}) - \cos(\vec{Q} \cdot \vec{T}_{31})}{\vec{Q} \cdot \vec{T}_{31}} \right].$$

Equation (5) is equivalent to Eq. (14b) of Wendelboe *et al.*,⁸ but even though its first two terms are regular, the last term has a singularity when $\vec{Q} \cdot \vec{T}_{31} \rightarrow 0$. When this limit is taken, we get

$$\mp \frac{iA\vec{Q} \cdot \hat{n}}{4\pi} e^{i\vec{Q} \cdot \vec{R}_0} \quad \text{if } \vec{Q} \cdot \vec{T}_{12} \rightarrow 0 \text{ and } \vec{Q} \cdot \vec{T}_{31} \rightarrow 0. \quad (6)$$

This demonstrates that these representations are not truly singular since they have finite limiting values, even though we have referred to them as having singularities. Our objective is to represent Eq. (4) by regular functions, so no limiting operations would be required. Relegating the details to Appendix A, we obtain the regular form of Eq. (4)

$$T = \mp \frac{A\vec{Q} \cdot \hat{n}}{4\pi} e^{i\vec{Q} \cdot \vec{R}_0} e^{ix/2} \{ \text{sinc}(z/2) [\text{sinc}(y/2) - \text{sinc}(y/4)\sin(y/4)] + 2\mathcal{D}(x, z) \}, \quad (7)$$

where

$$\begin{aligned} x &\equiv \vec{Q} \cdot \vec{T}_{12}, \\ y &\equiv \vec{Q} \cdot \vec{T}_{23}, \\ z &\equiv \vec{Q} \cdot \vec{T}_{31}, \end{aligned} \quad (8)$$

and the regular function \mathcal{D} is given by

$$\mathcal{D}(x, z) = \begin{cases} \frac{\text{sinc}(x/2) - \text{sinc}(z/2)}{x+z}, & (x+z) \neq 0, \\ 0, & (x+z) = 0. \end{cases} \quad (9)$$

Henceforth, we refer to Eq. (7) as the TriKirch model or simply TriKirch to indicate that it represents scattering from a triangle using the Kirchhoff approximation.

B. Time domain representation of a scattered signal

The scattered signal from an object for which the scattering amplitude is $T(\vec{k}, \vec{q}, \omega)$ can be written as

$$S(\hat{q}, \omega) = S_i(\hat{k}, \omega) T(\hat{k}, \hat{q}, \omega), \quad (10)$$

where $\vec{k} = \omega\hat{k}/c$, $\vec{q} = \omega\hat{q}/c$, $S_i(\hat{k}, \omega)$ is the incident signal in direction \hat{k} , \hat{q} is the direction of the scattered signal, ω is the circular frequency and c is the sound speed. The frequency representation developed in Sec. I can be used to obtain a time domain representation for the scattered signal via an inverse Fourier transform, as is done in Fawcett.⁵

$$s(t) = \frac{1}{\sqrt{2\pi}} \int_{-\infty}^{\infty} S_i(\omega) T(\omega) e^{-i\omega t} d\omega, \quad (11)$$

where angular dependences have been omitted for brevity. Equation (4) can be expanded to read

$$\begin{aligned} T(\omega) &= \pm \frac{A\hat{Q} \cdot \hat{n}}{2\pi\hat{Q} \cdot \vec{T}_{12}} \frac{ic}{\omega} \\ &\times \left[\frac{e^{i\omega\alpha_1}}{\hat{Q} \cdot \vec{T}_{31}} + \frac{e^{i\omega\alpha_2}}{\hat{Q} \cdot \vec{T}_{23}} - \frac{e^{i\omega\alpha_3}}{\hat{Q} \cdot \vec{T}_{31}} - \frac{e^{i\omega\alpha_3}}{\hat{Q} \cdot \vec{T}_{23}} \right], \end{aligned} \quad (12)$$

here $\hat{Q} = \hat{k} - \hat{q}$, and

$$\begin{aligned} \alpha_1 &= \hat{Q} \cdot \vec{R}_0/c, \\ \alpha_2 &= \hat{Q} \cdot (\vec{R}_0 + \vec{T}_{12})/c, \\ \alpha_3 &= \hat{Q} \cdot (\vec{R}_0 - \vec{T}_{31})/c. \end{aligned} \quad (13)$$

Using this expression for the scattering amplitude in Eq. (11), we get

$$s(t) = \pm \frac{Ac\hat{Q} \cdot \hat{n}}{2\pi\hat{Q} \cdot \vec{T}_{12}} \left[\frac{\bar{s}_i(t - \alpha_1)}{\hat{Q} \cdot \vec{T}_{31}} + \frac{\bar{s}_i(t - \alpha_2)}{\hat{Q} \cdot \vec{T}_{23}} - \frac{\bar{s}_i(t - \alpha_3)}{\hat{Q} \cdot \vec{T}_{31}} - \frac{\bar{s}_i(t - \alpha_3)}{\hat{Q} \cdot \vec{T}_{23}} \right], \quad (14)$$

$$s(t) = \pm \begin{cases} \frac{-Ac\hat{Q} \cdot \hat{n}}{2\pi\hat{Q} \cdot \vec{T}_{12}} \left[\frac{s_i(t - \alpha_1)}{c} - \frac{\bar{s}_i(t - \alpha_2)}{\hat{Q} \cdot \vec{T}_{23}} + \frac{\bar{s}_i(t - \alpha_3)}{\hat{Q} \cdot \vec{T}_{23}} \right], & \hat{Q} \cdot \vec{T}_{31} \rightarrow 0, \hat{Q} \cdot \vec{T}_{12} \neq 0, \hat{Q} \cdot \vec{T}_{23} \neq 0, \\ \frac{Ac\hat{Q} \cdot \hat{n}}{2\pi\hat{Q} \cdot \vec{T}_{12}} \left[\frac{s_i(t - \alpha_2)}{c} + \frac{\bar{s}_i(t - \alpha_1)}{\hat{Q} \cdot \vec{T}_{31}} - \frac{\bar{s}_i(t - \alpha_3)}{\hat{Q} \cdot \vec{T}_{31}} \right], & \hat{Q} \cdot \vec{T}_{23} \rightarrow 0, \hat{Q} \cdot \vec{T}_{12} \neq 0, \hat{Q} \cdot \vec{T}_{31} \neq 0, \\ \frac{Ac\hat{Q} \cdot \hat{n}}{2\pi\hat{Q} \cdot \vec{T}_{31}} \left[\frac{s_i(t - \alpha_1)}{c} + \frac{\bar{s}_i(t - \alpha_2)}{\hat{Q} \cdot \vec{T}_{31}} - \frac{\bar{s}_i(t - \alpha_3)}{\hat{Q} \cdot \vec{T}_{31}} \right], & \hat{Q} \cdot \vec{T}_{12} \rightarrow 0, \hat{Q} \cdot \vec{T}_{31} \neq 0, \hat{Q} \cdot \vec{T}_{23} \neq 0, \\ \frac{-A\hat{Q} \cdot \hat{n}}{4\pi c} s'_i(t - \alpha_1) & \text{if } \vec{Q} \cdot \vec{T}_{12} \rightarrow 0 \text{ and } \vec{Q} \cdot \vec{T}_{31} \rightarrow 0, \end{cases} \quad (16)$$

where $s'_i = ds_i/dt$. Note that the only way that \hat{Q} can be perpendicular to two edges is when it is perpendicular to the plane of the triangle according to the identity $\hat{Q} \cdot (\vec{T}_{12} + \vec{T}_{23} + \vec{T}_{31}) = 0$. The scattered signal for the entire object is obtained by adding the scattered time series for all triangles. The details of the derivation leading to Eqs. (14) and (16) are provided in Appendix B.

III. VALIDATION AND EXAMPLES

The model developed in this paper approximates the Kirchhoff scattering integral on the surface of the scatterer; and its accuracy is judged based on how well it agrees with the Kirchhoff approximation. To test its accuracy, we apply it to cases for which the Kirchhoff approximation has analytic or close form solutions. This way the possibility of numerical error in the reference solution is minimized. In this section, we validate TriKirch for a square plate, a circular plate, a finite cylinder and a sphere. The shape of these objects systematically become more complex starting with a flat object with straight edges, a flat object with a curved edge, a curved object with zero Gaussian curvature and finally a curved object with positive Gaussian curvature.

A. Square plate

The analytic expression from Eq. (2) for a square plate of dimension a , centered on the xy -plane is given by

$$T = \mp \frac{i}{4\pi} a^2 Q_z \text{sinc}(aQ_x/2) \text{sinc}(aQ_y/2). \quad (17)$$

Since the square plate can be exactly represented by as few as two triangles, this case is the simplest application of

where

$$\bar{s}(t) = \int_{-\infty}^t s(\tau) d\tau. \quad (15)$$

If any quantity in the denominators in Eq. (14) goes to zero, appropriate limits must be taken to express it in finite form. Equation (14) for these cases is given by

TriKirch, and as expected, its results shown in Fig. 2 exactly agree with those obtained from Eq. (17). In Fig. 2 the scattering amplitude is computed for an incident plane wave along the z axis as a function receiver location measured by angle ϑ . For this example, $a = 1$ m and $ka = 20$.

B. Circular plate

The analytic solution of Eq. (2) for a circular plate of radius a on the xy -plane is given by

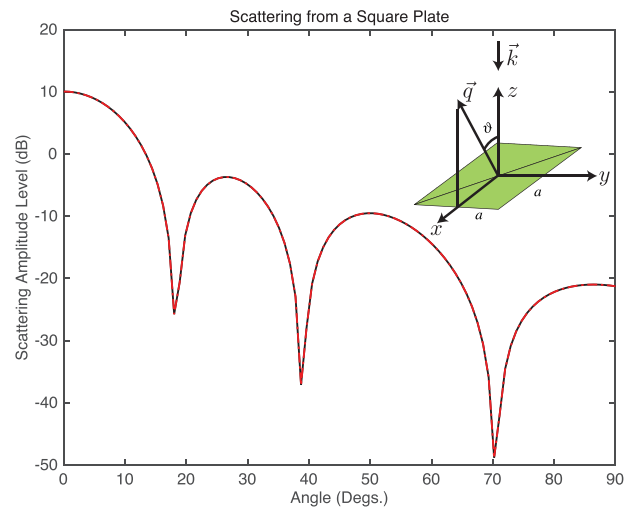


FIG. 2. (Color online) The scattering amplitude as a function of receiver angle for a square plate. The solid line shows the results from Eq. (17) and the broken line shows the results from TriKirch. The inset show the two triangles on the plate and the scattering geometry.

$$T = \mp \frac{ia^2 Q_z}{2} \frac{J_1\left(a\sqrt{Q_x^2 + Q_y^2}\right)}{a\sqrt{Q_x^2 + Q_y^2}}, \quad (18)$$

where J_1 is the Bessel function of order 1. Application of TriKirch to a plate with curved edges requires enough triangles to approximate the curved edge with straight lines. The results shown in Fig. 3 are for $a=0.5$ m and for a plane wave incident along the negative z axis at frequency corresponding to $ka=10$. The top left panel in Fig. 3 shows a comparison of the scattering amplitude computed using Eq. (18) and TriKirch as a function of the receiver angle measured from the z axis for the case when five elements per wavelength at $ka=10$ is used to mesh the surface. This implies that the edges of the triangles making up the surface have an average length of less than $\lambda/5$. The top panel on the right shows a comparison of the scattering amplitude for the same two models as a function of ka for a fixed receiver angle of 30° . The bottom two panels are the same results as the top two panels for a finer mesh of ten elements per wavelength. Figure 3 shows that the TriKirch results agree almost perfectly with the analytic solution even for a coarse mesh of five elements per wavelength and the agreement gets better for the finer mesh. Furthermore, the two panels on the right show almost identical agreement between the two models up to $ka=50$, while the plate is meshed at only ten elements per wavelength at $ka=10$. This shows that for a planar scatterer with curved edges the accuracy of TriKirch depends more on whether the curved edge is approximated accurately by straight lines rather than the operating frequency.

C. Finite cylinder

For a finite cylinder of length L and radius a Eq. (2) can be evaluated in closed form when the axis of the cylinder is on the plane of incidence, i.e., when both \vec{k} and \vec{q} lie on a plane containing the axis of the cylinder

$$T = \pm \frac{ik\alpha La}{4\pi} \text{sinc}\left(\frac{k\beta L}{2}\right) \Gamma(k\alpha a), \quad (19)$$

where

$$\Gamma(x) = \pi(-iJ_1(x) + \mathbf{H}_{-1}(x)).$$

In the above equations $\alpha = \sin\theta_i + \sin\theta_s$, $\beta = \cos\theta_i + \cos\theta_s$, θ_i is the incident angle, θ_s is the scattered angle, both measured from the axis of the cylinder, $\mathbf{H}_{-1}(x)$ is Struve function defined by⁹

$$\mathbf{H}_\nu(z) = \frac{2(z/2)^\nu}{\sqrt{\pi}\Gamma(\nu + 1/2)} \int_0^1 (1-t^2)^{\nu-1/2} \sin(zt) dt.$$

In deriving Eq. (19) only the illuminated region of the surface is included in the integration, as is required by the Kirchhoff approximation. Figure 4 shows a comparison of scattering from a finite cylinder computed using Eq. (19) and TriKirch for $L=5$ m and $a=0.5$ m. In this example a 2 kHz plane wave is incident at 45° and the receiver is sweeping the angle ϑ from zero to 180° . All angles are measure from the axis of the cylinder. The scattering amplitude as a function of frequency computed using Eq. (19) and TriKirch is shown in Fig. 5. In this simulation, the incident field is perpendicular to and the scattered angle makes a 60° with the axis of the cylinder. This results in interference patterns

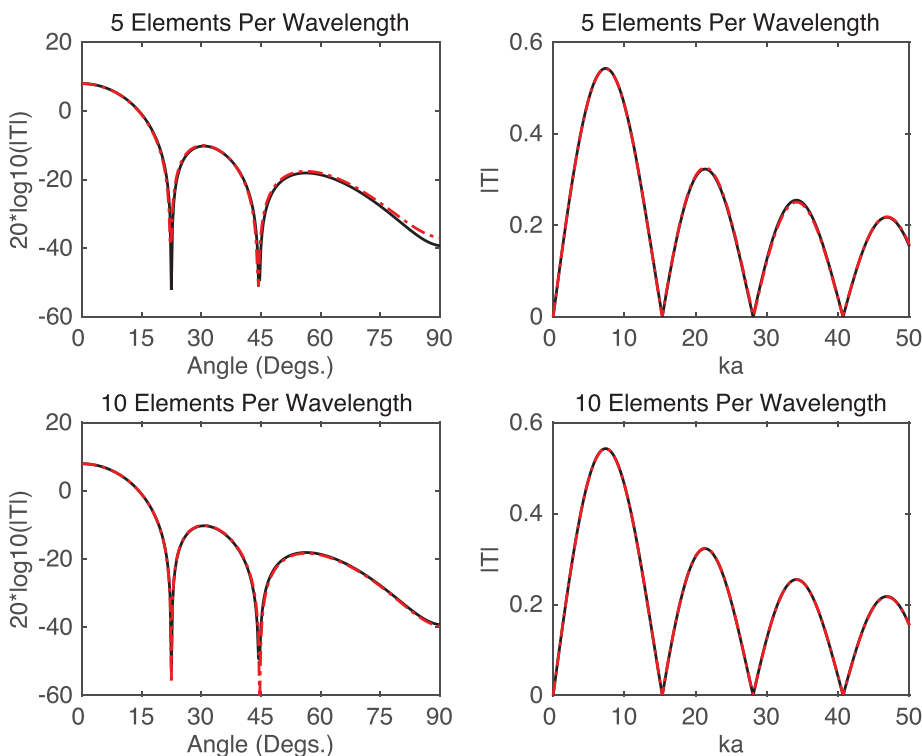


FIG. 3. (Color online) This figure shows scattering from a circular plate of radius 0.5 m computed by Eq. (18) in solid lines and TriKirch in broken lines. The incident field is a plane wave in the negative z direction. The top left panel shows the scattering amplitude as a function of receiver angle measured from the z axis. The top right panel shows the scattering amplitude as a function of ka for a fixed receiver angle of 30° . In the top two panels the plate is meshed at five element per wavelength at $ka=10$. In the bottom two panels the computation is repeated for a finer mesh of ten elements per wavelength.

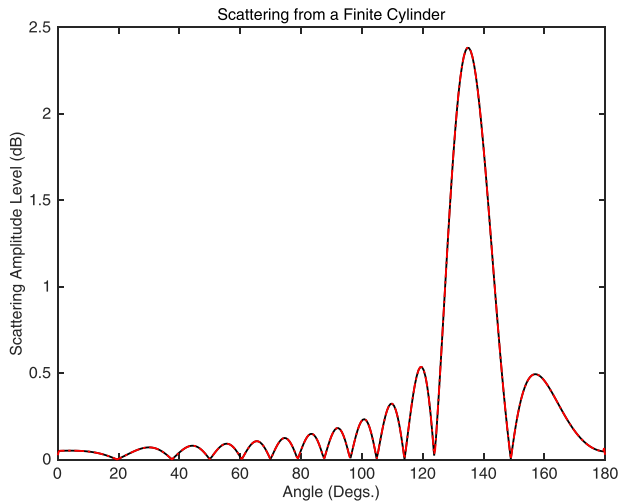


FIG. 4. (Color online) The scattering amplitude as a function of receiver angle for a finite cylinder. The solid line shows the results from Eq. (19) and the broken line shows the results from TriKirch.

whose nulls are 600 Hz apart. The top panel in this figure shows the scattering amplitude as a function of frequency for the case when the cylinder is meshed at ten elements per wavelength at a frequency of 2 kHz. This translates to a wavelength of 75 cm in water and triangles whose average edge lengths do not exceed 7.5 cm, resulting in 6560 triangles to mesh the entire cylinder. The bottom panel shows the same results for a finer mesh of triangles whose average edge lengths do not exceed 15 mm, resulting in 163 500 triangles. These results show that TriKirch requires a minimum of ten elements per wavelength of the frequency of interest to produce accurate results. It is interesting to note that TriKirch produces more accurate results than those obtained by using the second-order stationary phase method to evaluate Eq. (2). This is shown in Fig. 6, where the stationary phase solution is included in addition to the results shown in

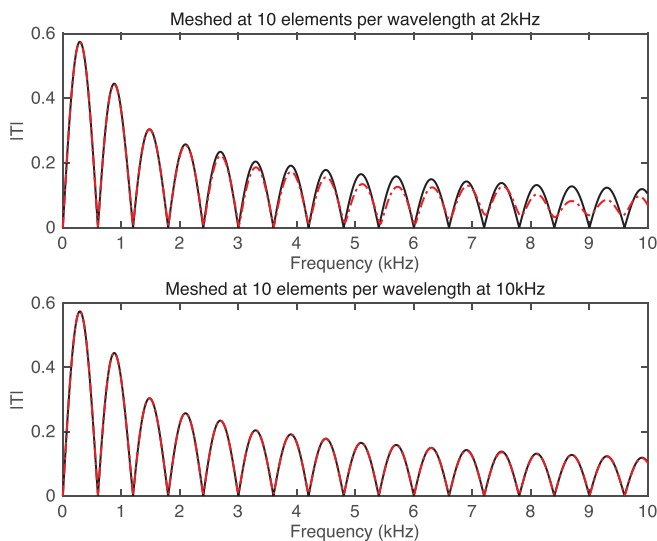


FIG. 5. (Color online) The scattering amplitude as a function of frequency for a finite cylinder. The solid line shows the results from Eq. (19) and the broken line shows the results from TriKirch. In the top panel the cylinder is meshed at ten elements per wavelength at a frequency of 2 kHz and in the bottom panel it is meshed at ten elements per wavelength at a frequency of 10 kHz.

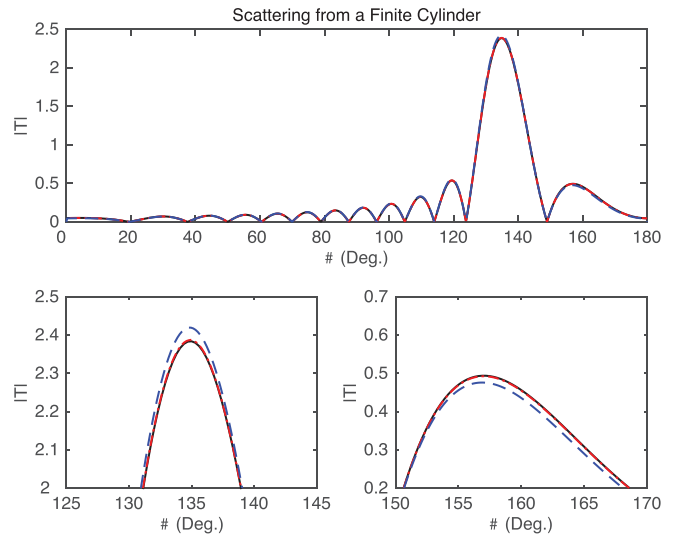


FIG. 6. (Color online) The scattering amplitude as a function of receiver angle for a finite cylinder. The solid line shows the results from Eq. (19), the broken line shows the results from TriKirch and the dashed line shows the results for the stationary phase solution. The bottom two panels show a close-up of the results near 135° and 157°.

Fig. 4. While the TriKirch solution shows excellent agreement with those obtained from Eq. (19), the stationary phase solution shows small differences for all angles, particularly near specular (135°) and 157°. This shows that even the second-order stationary phase method cannot approximate the Kirchhoff integral as well as TriKirch. A close-up of the results near these angles is shown in the bottom two panels.

D. Sphere

The scattering amplitude for a sphere of radius a in the backscattered direction can be obtained from Eq. (2) analytically,

$$T = \mp \frac{iae^{-2ika}}{4ka} (e^{2ika} - 2ika - 1). \quad (20)$$

A comparison of scattering amplitude for a sphere of $a = 0.25$ m computed using TriKirch and the above formula as a function of the dimensionless parameter ka is shown in Fig. 7. In the TriKirch computation eight elements per wavelength at the maximum ka of 20 were used to mesh the sphere, which resulted in 19596 triangles. Figure 7 shows that there is excellent agreement between the two solutions.

As an example of the time domain application of TriKirch, we used Eqs. (14) and (16) to compute the scattering of a Ricker wavelet, with a center frequency of 445 kHz, from a 10 cm rigid sphere. For a rigid sphere, the lower signs in the above equations were used. This is the example that was also presented in Wendelboe *et al.*⁸ The results are shown in Fig. 8, where the solid lines are for the exact partial wave solution for the rigid sphere and the broken lines are for the TriKirch solutions. The top panels are for the case when the sphere was meshed at six elements per wavelength ($\lambda = 3.4$ mm). This resulted in 967 000 triangles with an average area of 0.13 mm². The bottom two panels are for the case when the sphere was meshed at one element per wavelength, resulting in 13 600 triangles with an average area of 9.2 mm².

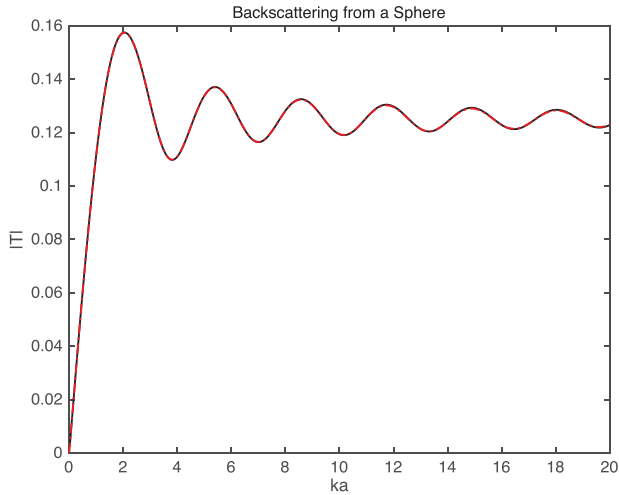


FIG. 7. (Color online) The scattering amplitude in the backscattered direction as a function of ka for a sphere of radius 0.25 m computed using Eq. (20) in solid line and TriKirch in broken line.

In both cases there is excellent agreement between the TriKirch and the reference solutions, even for the coarser mesh the figure has to be magnified to discern the differences between the two solutions. As was pointed out by Wendelboe *et al.*,⁸ the oscillations seen in the top right panel of Fig. 8 are as a result of surface discretization, but it is curious that in the solution by Wendelboe *et al.*⁸ solution they are clearly visible, while in our solution they are much smaller, even though their mesh size of 11 mm² is close to our mesh size of 9.2 mm².

IV. SUMMARY

In this paper, we derived frequency and time domain expressions for the scattering of acoustic waves from an

arbitrarily shaped object. In the frequency domain, we derived the scattering amplitude for a single triangle analytically and obtained the scattering amplitude for a triangularly meshed object by coherently summing the contributions from all the triangles that make up its surface. In the time domain, we used the inverse Fourier transform on the frequency domain result to obtain an analytic expression for the scattering of a signal from a single triangle and used it to compute the scattered signal from the entire object by adding the scattered signals for all triangles. Unlike previous results, the frequency domain representation is free of singularities and a single formula can be used under any condition. In the time domain, we derived singularity-free formulas for all possible cases in which singularities can occur. We validated both formulations by applying them to various problems for which well-known solutions exist. In order of increasing complexity, they include the square plate, the circular plate, the finite cylinder and the sphere.

On the basis of how the model is developed, its validation for the simple targets in this paper guarantees that it can compute scattering from any arbitrarily shaped, non-penetrable target to the accuracy of the Kirchhoff approximation, as long as the target is adequately meshed. Like the Kirchhoff approximation, it treats scattering locally, so it does not account for multiple scattering from different facets on the surface of the target. However, this can be done by using a ray model that determines when a ray hits a surface facet and uses TriKirch to compute the scattered ray. Similarly, to handle scattering from a target in a waveguide, the total scattering amplitude should be computed as the sum of scattering amplitudes for all combinations of pairs of incident and scattered rays.

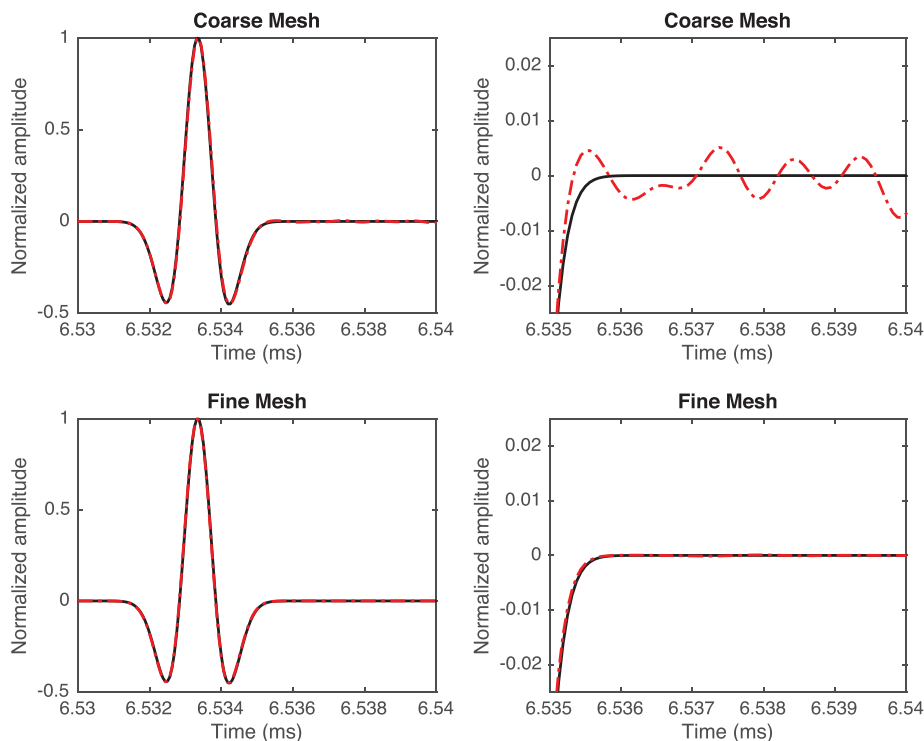


FIG. 8. (Color online) The scattering of a Ricker wavelet from a rigid sphere. The reference solution is the exact partial wave solution in solid lines and the TriKirch solutions are in broken lines. The top two panels are for a mesh size of one element per wavelength and the bottom two panels are for a mesh size of six element per wavelength. The figures on the right column are blowups of the solutions on the left column to reveal the differences between the TriKirch and the reference solutions.

ACKNOWLEDGMENTS

This work was partly supported by the Office of Naval Research Contract No. N00014-10-C-0440.

APPENDIX A: THE DERIVATION OF EQ. (7)

Consider Eq. (4),

$$T(\vec{k}, \vec{q}) = \mp \frac{A\vec{Q} \cdot \hat{n}}{2\pi} e^{i\vec{Q} \cdot \vec{R}} e^{i\vec{Q} \cdot \vec{T}_{12}/2} T_1(\vec{k}, \vec{q}), \quad (\text{A1})$$

where

$$T_1 = \frac{\left(e^{-i(z/2)} \text{sinc} \frac{x+z}{2} - e^{(x+z)/2} \text{sinc} \frac{z}{2} \right)}{x}, \quad (\text{A2})$$

$$T_2 = \frac{-2x \cos((x+z)/2) \text{sinc}(z/2) + 2z(\sin((x+z)/2) \cos(z/2) - \cos((x+z)/2) \sin(z/2))}{xz(x+z)}. \quad (\text{A5})$$

The trigonometric identities for the products of sines and cosines can be used to combine the second term in the numerator of Eq. (A5). This and further manipulations result in

$$T_2 = \frac{\text{sinc}(x/2)}{(x+z)} - \frac{\cos((x+z)/2) \text{sinc}(z/2)}{(x+z)}. \quad (\text{A6})$$

Using the identity

$$\cos((x+z)/2) = 1 - 2 \sin^2((x+z)/4),$$

in Eq. (A6) gives

$$T_2 = \frac{\text{sinc}(x/2)}{(x+z)} - \frac{(1 - 2 \sin^2((x+z)/4)) \text{sinc}(z/2)}{(x+z)}.$$

The above equation can be rewritten as

$$T_2 = \mathcal{D}(x, z) + \frac{2 \sin^2((x+z)/4) \text{sinc}(z/2)}{(x+z)}, \quad (\text{A7})$$

where $\mathcal{D}(x, z)$ is defined in Eq. (9). The second term can be written as

$$\frac{1}{2} \text{sinc}((x+z)/4) \text{sinc}(z/2) \text{sinc}((x+z)/4),$$

resulting in the final expression

$$T = \mathcal{D}(x, z) + \frac{1}{2} \text{sinc}((x+z)/4) \text{sinc}(z/2) \text{sinc}((x+z)/4) + \frac{i}{2} \text{sinc}(z/2) \text{sinc}((x+z)/2). \quad (\text{A8})$$

and x , y , and z have been defined in Eq. (8). The above expression can be simplified to give

$$T_1 = T_2 + \frac{i}{2} \text{sinc}(z/2) \text{sinc}((x+z)/2), \quad (\text{A3})$$

where

$$T_2 = \frac{-2 \cos((x+z)/2) \text{sinc}(z/2)}{xz} + \frac{2 \cos(z/2) \text{sinc}((x+z)/2)}{x(x+z)}. \quad (\text{A4})$$

It is obvious that the singularity is in T_2 as the last term in Eq. (A3) is regular. The two terms in T_2 can be combined to give

Substituting the above expression in Eq. (A1) and using Eq. (8) for x , y and z gives Eq. (7). It is obvious that the singularity in Eq. (A8) is in $\mathcal{D}(x, z)$. However, $\mathcal{D}(x, z)$ is perfectly well-behaved once it is understood that it goes to zero when $(x+z) \rightarrow 0$. To inspect the behavior of $\mathcal{D}(x, z)$ for small $(x+z)$, let $\Delta = x+z$, then

$$\lim_{\Delta \rightarrow 0} \mathcal{D}(\Delta - z, z) = \frac{-z \cos(z/2) + 2 \sin(z/2)}{z^2} + O(\Delta).$$

The above expression is perfectly well-behaved for any z except $z=0$, but when $z \rightarrow 0$, we get

$$\lim_{z \rightarrow 0} \frac{-z \cos(z/2) + 2 \sin(z/2)}{z^2} = \frac{z}{12} + O(z^3).$$

The same arguments can be applied when $x \rightarrow 0$, verifying Eq. (9).

APPENDIX B: THE DETAILS OF THE DERIVATION LEADING TO EQS. (14) AND (16)

Consider the inverse Fourier transform of a single term in Eq. (12),

$$u(t) = \frac{1}{\sqrt{2\pi}} \int_{-\infty}^{\infty} \frac{i}{\omega} S_i(\omega) e^{-i\omega(t-\alpha_1)} d\omega. \quad (\text{B1})$$

Taking the time derivative of the above equation gives

$$\frac{du(t)}{dt} = \frac{1}{\sqrt{2\pi}} \int_{-\infty}^{\infty} S_i(\omega) e^{-i\omega(t-\alpha_1)} d\omega = s(t - \alpha_1),$$

where $s(t)$ is defined in Eq. (11). This leads to

$$u(t) = \int_{-\infty}^t s(\tau - \alpha_1) d\tau = \bar{s}(t - \alpha_1),$$

where $\bar{s}(t)$ is defined in Eq. (15). The use of Eq. (B1) in every term in Eq. (12) leads to Eq. (14).

For the case when $\hat{Q} \cdot \vec{T}_{31} \rightarrow 0$, but $\hat{Q} \cdot \vec{T}_{23}$ and $\hat{Q} \cdot \vec{T}_{12}$ are nonzero, the relevant part of Eq. (12) can be written

$$\lim_{\hat{Q} \cdot \vec{T}_{31} \rightarrow 0} \frac{ic}{\omega} \left[\frac{e^{i\omega\alpha_1}}{\hat{Q} \cdot \vec{T}_{31}} - \frac{e^{i\omega\alpha_3}}{\hat{Q} \cdot \vec{T}_{31}} \right] = -e^{i\omega\alpha_1},$$

where Eq. (13) has been used. Applying Eq. (11) to this piece results in

$$\frac{-1}{\sqrt{2\pi}} \int_{-\infty}^{\infty} S_i(\omega) e^{-i\omega(t-\alpha_1)} d\omega = -s(t - \alpha_1).$$

Substituting the right hand side of this equation in Eq. (14) gives the top equation in Eq. (16). A similar analysis results in the second equation in Eq. (16).

For the case when $\hat{Q} \cdot \vec{T}_{12} \rightarrow 0$, but $\hat{Q} \cdot \vec{T}_{23}$ and $\hat{Q} \cdot \vec{T}_{31}$ are nonzero, Eq. (12) can be written

$$T(\omega) = \pm \frac{A\hat{Q} \cdot \hat{n}}{2\pi\delta} \frac{i}{\omega c} e^{i\omega\alpha_1} \left[\frac{1}{a} - \frac{e^{i\omega\delta}}{a+\delta} - \frac{e^{-i\omega a}}{a} + \frac{e^{-i\omega a}}{a+\delta} \right], \quad (\text{B2})$$

where $\delta = \hat{Q} \cdot \vec{T}_{12}/c$, $a = \hat{Q} \cdot \vec{T}_{31}/c$ and use has been made of Eq. (13) and $\vec{T}_{12} + \vec{T}_{23} + \vec{T}_{31} = 0$. The quantity in square brackets can be expanded in a series involving powers of δ ,

$$\left(\frac{1}{a^2} - \frac{i\omega}{a} - \frac{e^{-i\omega a}}{a^2} \right) \delta + O(\delta^2).$$

Thus in the limit when $\delta \rightarrow 0$, Eq. (B2) becomes

$$T(\omega) = \pm \frac{A\hat{Q} \cdot \hat{n}}{2\pi} \frac{i}{\omega c a} e^{i\omega\alpha_1} \left[\frac{1}{a} - i\omega - \frac{e^{-i\omega a}}{a} \right]. \quad (\text{B3})$$

Applying Eq. (11) to the above equation, substituting for a and remembering that in this limit $\alpha_1 = \alpha_2$, gives the third equation in Eq. (16).

Finally, when both $\hat{Q} \cdot \vec{T}_{21} \rightarrow 0$ and $\hat{Q} \cdot \vec{T}_{31} \rightarrow 0$, we take the limit of Eq. (B3) when $a \rightarrow 0$, which results in

$$T(\omega) = \pm \frac{A\hat{Q} \cdot \hat{n}}{4\pi} \frac{i\omega}{c} e^{i\omega\alpha_1}. \quad (\text{B4})$$

Applying Eq. (11) to this equation gives

$$s(t) = \pm \frac{A\hat{Q} \cdot \hat{n}}{4\pi} \frac{i}{c} \frac{1}{\sqrt{2\pi}} \int_{-\infty}^{\infty} \omega S_i(\omega) e^{-i\omega(t-\alpha_1)} d\omega,$$

which can be written as

$$s(t) = \pm \frac{-A\hat{Q} \cdot \hat{n}}{4\pi c} s'(t - \alpha_1), \quad (\text{B5})$$

where

$$s'(t - \alpha_1) = \frac{1}{\sqrt{2\pi}} \frac{d}{dt} \int_{-\infty}^{\infty} S_i(\omega) e^{-i\omega(t-\alpha_1)} d\omega.$$

Equation (B5) is the last equation in Eq. (16).

¹M. Born and E. Wolf, *Principles of Optics*, 6th ed. (Pergamon Press, New York, 1980), pp. 378–382.

²J. Perez and M. F. Catedra, "Applications of physical optics to the rcs computation of bodies modeled with nurbs surfaces," *IEEE Trans. Antennas Propag.* **42**, 1404–1411 (1994).

³G. S. Sammelman, "Propagation and scattering in very shallow water," *Proc. IEEE Oceans* **1**, 337–344 (2001).

⁴O. George and R. Bahl, "Simulations of backscattering of high frequency sound from complex objects and sea bottom," *IEEE J. Ocean Eng.* **20**, 119–130 (1995).

⁵J. A. Fawcett, "Modeling of high frequency scattering from objects using a hybrid Kirchhoff/diffraction approach," *J. Acoust. Soc. Am.* **109**(4), 1312–1319 (2001).

⁶R. Dashen and D. Wurmser, "A new theory for scattering from a surface," *J. Math. Phys.* **32**(4), 971–985 (1991).

⁷R. Dashen and D. Wurmser, "Approximate representation of the scattering amplitude," *J. Math. Phys.* **32**(4), 986–996 (1991).

⁸G. Wendelboe, F. Jacobsen, and J. M. Bell, "A numerically accurate and robust expression for bistatic scattering from a plane triangular facet," *J. Acoust. Soc. Am.* **119**(2), 701–704 (2006).

⁹M. Abramowitz and I. A. Stegun, *Handbook of Mathematical Functions* (Dover Publications, New York, 1972).